A PRACTICAL DATA-DRIVEN APPROACH FOR PRECISE STEM WATER POTENTIAL MONITORING IN PISTACHIO AND ALMOND ORCHARDS USING SUPERVISED MACHINE LEARNING ALGORITHMS

Mehrad Mortazavi[1], **Stefano Carpin**[2], **Arash Toudeshki**[1], **Reza Ehsani**[1*]

[1] Department of Mechanical Engineering, University of California, Merced, USA
[2] Department of Computer Science and Engineering, University of California, Merced, USA

ABSTRACT

The advent of machine learning technologies in conjunction with the advancements in UAV-based remote sensing pioneered a new era of research in agriculture. The escalating concern for water management in drought-prone areas such as California underscores the urgent need for sustainable solutions. Stem water potential (SWP) measurement using pressure chambers is one of the most common methods used to directly determine tree water status and the optimal timing for irrigation in orchards. However, this approach is inefficient due to its labor-intensive nature. To address this problem, we used weather, thermal and multispectral data as inputs to the machine learning (ML) algorithms to predict the SWP of pistachio and almond trees. For each crop, we first deployed six supervised ML classification models: Random Forest (RF), Support Vector Machine (SVM), Gaussian Naive Bayes (GNB), Decision Tree (DT), K-Nearest Neighbors (KNN), and Artificial Neural Network (ANN). All classifiers provided more than 79% of accuracy while RF showed high performance in both pistachio and almond orchards at 88% and 89%, respectively. The feature importance results by the RF model revealed that the weather features were the most influential factors in the decision-making process. In both crops, canopy temperature T_c was the next important feature closely followed by OSAVI in pistachios and NDVI in almonds. RF regression model predicted SWPs with R^2 of 0.70 in pistachio and R^2 of 0.55 in the almond orchard. Our results demonstrate that ML models are practical tools for irrigation scheduling decisions. This study offered a data-driven approach that effectively balances minimal data requirements with accuracy to facilitate optimal water management for end-users.

Keywords: *Machine learning, Data fusion, Water stress, Stem water potential, Remote sensing*

*E-mail address: rehsani@ucmerced.edu

1 INTRODUCTION

The state of California is a major crop producer in the world (Hong et al., 2020). California's agricultural exports achieved a value of $22.5 billion in 2021, showing a 20% percent growth over the span of 10 years. The foundation of this success rests on the state's almond and pistachio industries that contribute to about 30% of these exports in value according to CFDA reports. However, crop production in California is subject to substantial uncertainty due to high vulnerability to drought and water shortage (Medellín-Azuara et al., 2022). In 2014, California adopted the Sustainable Groundwater Management Act (SGMA) regulations to mitigate groundwater overdraft, especially in agriculture (Espinoza et al., 2023). These regulations aim to optimize water allocation and reduce wastage. Guidelines cover aspects such as irrigation scheduling and water application methods. With these regulations in effect, the need for efficient irrigation methods become more important (Escriva-Bou et al., 2020). The escalation in crop water requirements is urging growers to explore new irrigation strategies that can accommodate severe drought conditions. It is crucial to seek solutions that are not labor-intensive and time-consuming to allow for efficient water management under challenging circumstances (Kagan et al., 2022).

Stem water potential (SWP) is a direct measure of tree water level. SWP measurement has been exclusively used in the field of horticulture and viticulture for irrigation scheduling and high-quality crop production (Ohana-Levi et al., 2022; Carrasco-Benavides et al., 2022). In commercial orchards where SWP is monitored, irrigation adjustments are made according to the average SWP measurement from a group of selected trees. However, manual SWP measurement is labor-intensive and not practical for evaluating the water status of all trees within a large-scale orchard (Giménez-Gallego et al., 2021). To address the limitations associated with ground measurements, remote sensing using unmanned aerial vehicles (UAVs) has emerged as a promising solution for predicting SWP to provide rapid and efficient assessments. Remote sensing can leverage spectral data to facilitate the identification of crop water status (Gautam and Pagay, 2020; Romero et al., 2018). Supplementary information such as soil water content (SWC), local weather data, and evapotranspiration (ET) can synergistically be used along with spectral measurements to enhance the accuracy of SWP predictions.

Various studies have investigated thermal and multispectral UAV imagery to assess tree water status.UAV-based Normalized difference vegetation index (NDVI) and crop water stress index (CWSI) were compared with water status indicators including SWP to detect water stress in almond cultivars (Gutiérrez-Gordillo et al., 2021). CWSI was measured using high- and low-resolution UAV thermal imaging to estimate midday SWP and stomatal conductance in cherry cultivars (Carrasco-Benavides et al., 2020). Thermal and multispectral UAV imaging using a high-end all-in-one camera was conducted to establish a relationship between VIs and crop quality in Pistachios (Martínez-Peña et al., 2023). While both NDVI and CWSI were capable of detecting water stress, CWSI exhibited higher sensitivity. CWSI value of 0 represents a crop with no stress and a value of 1 indicates non-transpiring crops that are under severe water stress. Studies have offered various approaches to compute the CWSI (Idso et al., 1981; Egea et al., 2017; Kirnak et al., 2019; Liu et al., 2022). The main difference between various methods is often found in the computation of the lower and upper limits. For instance, a widely used approach offered by (Idso et al., 1981), also referred to as the empirical approach, is to determine the lower limit as a linear function of vapor pressure deficit (VPD). The upper boundary can be calculated either by taking the maximum observed difference between the canopy and air temperatures or through a linear relationship the vapor pressure gradient (VPG), as described by (Katimbo et al., 2022). Some studies have discussed the use of constant values (e.g 5°C) for the calculation upper baselines (Ben-Gal et al., 2009). One limitation of CWSI calculation is that it requires specific adjustments according to the lower and upper limits for the difference between canopy temperature and air temperature (González-Dugo et al., 2014). Its reliance on experimental data to establish lower or upper baselines can be significantly affected by changes in weather conditions. This variability raises concerns about its applicability for real-time irrigation scheduling and the adaptability of the established baseline across different climate zones (Katimbo et al., 2022).

The utilization of machine learning (ML) in remote sensing has been on the rise over the past decade (Virnodkar et al., 2020). These ML-powered technologies are actively deployed to automate the process of data exploration and address information deficits across spatial and temporal dimensions (Benos et al., 2021; Sun and Scanlon, 2019; Marques Ramos et al., 2020). ML algorithms excel in capturing complex and nonlinear interactions between multiple input variables to predict desired outputs. They can effectively utilize fundamental components as inputs to reduce the dependency on carefully engineered features or variables with high potential correlations to the target output. This capability allows ML models to identify intricate patterns in the data and offers a more flexible data-driven approach compared to traditional methods that often require significant feature engineering. Several studies have used ML algorithms to predict plant water status and more exclusively SWP. In one study, boosted regression trees (BRT) algorithm was used to predict SWP in grapevine. Correlation of $r = 0.9$ between SWP and input variables among which leaf temperature displayed higher importance, was achieved (Ohana-Levi et al., 2022). Hyperspectral imageries from grape leaves were analyzed using Random Forest (RF) and Extreme Gradient Boosting (XGBoost) to classify water-stressed leaves based on their SWP values with $\%84$ accuracy (Loggenberg et al., 2018). Multiple ML models were deployed to predict olive SWP using various multi-spectral vegetation indices and spectral bands with RF outperforming other models with $R^2 = 0.78$ (Garofalo et al., 2023). Normalized difference red edge index (NDRE), SWC, and ET were used to predict raw SWP values in an almond orchard using RF and Artificial Neural Networks (ANN). Together, all models resulted in an average $R^2 = 0.73$ and $RMSE = 2.5bars$ for SWP prediction in almond (Savchik et al., 2024). SWP, along with SWC and atmospheric features, have also been used as input variables to predict the leaf temperature as an indicator of almond water status. In this study, ANN was able to predict the target with $R^2 = 0.78$ (Meyers et al., 2019). Currently, there are limited studies in almonds and especially pistachios where ML is used to predict direct indicators of tree water status such as SWP.

There remains an opportunity to carve out a pathway toward a simplified, cost-effective, and non-destructive approach to remotely determine SWP and facilitate its adoption by the end-users. The motivation for such an approach emerges from the necessity to integrate emerging technologies into current field practices, particularly for large-scale orchard water management, where precise monitoring of tree water status forms an integral component of efficient irrigation. Tree water status has been estimated by an array of direct and indirect methodologies, ranging from sap flow sensors (Mobe et al., 2020; Alizadeh et al., 2021), soil moisture sensors(Vera et al., 2019; Millán et al., 2020), and dendrometers (Celedón et al., 2012) to hyperspectral and multispectral sensors (Ballester et al., 2018; Zhao et al., 2017; Zhou et al., 2021). Although these techniques have demonstrated effectiveness in assessing crop water status, those of which require ground installation or measurement, typically involve intrusive procedures and can impose significant financial and labor burdens, especially in large commercial orchards. Moreover, conventional techniques might not sufficiently capture the spatial and temporal heterogeneity of SWP within the tree and across the orchard.

Most orchard infrastructures are not designed to support tree-specific irrigation; however, some systems allow irrigation to be controlled per block. By gaining insights into specific stress levels of trees, growers could make more informed decisions. This would enable them to prioritize irrigation in blocks with higher numbers and greater severity of water stress. Given the rapid advancements in remote sensing technology and machine learning, there is an opportunity to leverage these developments to enhance SWP prediction. The adoption of a predictive model predominantly reliant on remotely sensed and weather data, unites the power of aerial imaging technology with the sophistication of data-driven algorithms, representing a logical progression in this domain. In this study, our objective was to develop a data-driven model that balances minimal data requirements with accuracy while enabling practical utility for end-users in managing orchard irrigation scheduling. We used six ML classifiers and deployed weather, thermal, and multispectral variables to predict SWP categories of each tree in almond and pistachio orchards, as seen in Figure 1. Additionally, RF regression and classification models were used to determine the SWP prediction performance using different features. Here, we present a practical and cost-effective approach for tree-specific water status detection in orchards.

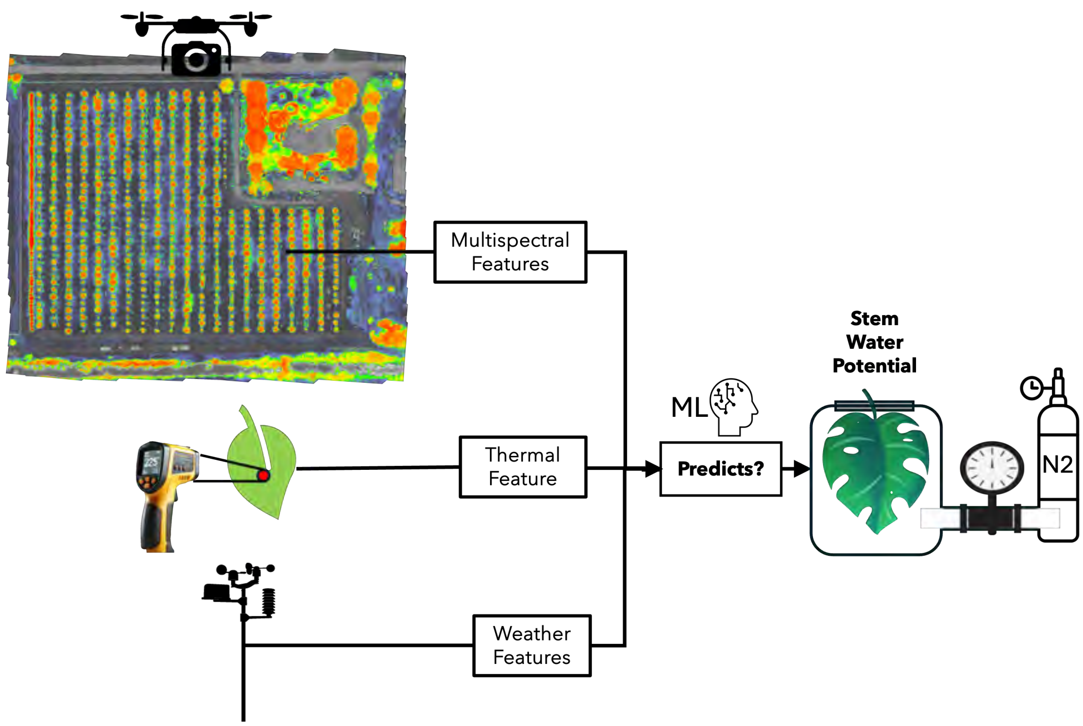

FIGURE 1: Flowchart of the research investigating whether machine learning can predict stem water potential in pistachio and almond orchards.

2 MATERIALS AND METHODS

2.1 Experimental Sites

The study sites include a 2.5-ha (6.1 acres) pistachio orchard (PO) and a 3-ha (7.4 acres) almond orchard (AO) situated in Merced County, within California's San Joaquin valley as shown in Figure 2. This region is known for its Mediterranean climate, characterized by hot and dry summers and mild and wet winters. The pistachio variety was Kerman, and the trees were 9 years old. The almond was a nonpareil variety and trees were 12 years old.

The average maximum and minimum temperatures in Merced, CA, between June and August 2022 were 36°C (97°F) and 12°C (54°F), respectively. The PO was irrigated through a double-line drip irrigation system, while the almond orchard was irrigated through a macro jet irrigation system. A total of 14 data collection field trips were conducted between June and August 2022. These data collections trips were evenly split between PO and AO, with seven experiments in each orchard. For PO these days were: June 7, June 21, July 5, July 13, July 26, August 2, August 12 representing day of year (DOY) 158, 172, 186, 194, 207, 214, 224, respectively. For AO these days were: June 8, June 23, July 8, July 15, July 30, August 3, August 31 representing day of year (DOY) 159, 174, 189, 196, 211, 215, 243, respectively. A total of 18 trees in the PO and 17 trees in the AO were selected as sample trees from which stem water potential (SWP), leaf temperature, and aerial multispectral images were collected. In each field, the sample trees were randomly chosen in blocks of three or four across the fields to account for the possible variability in the orchards.

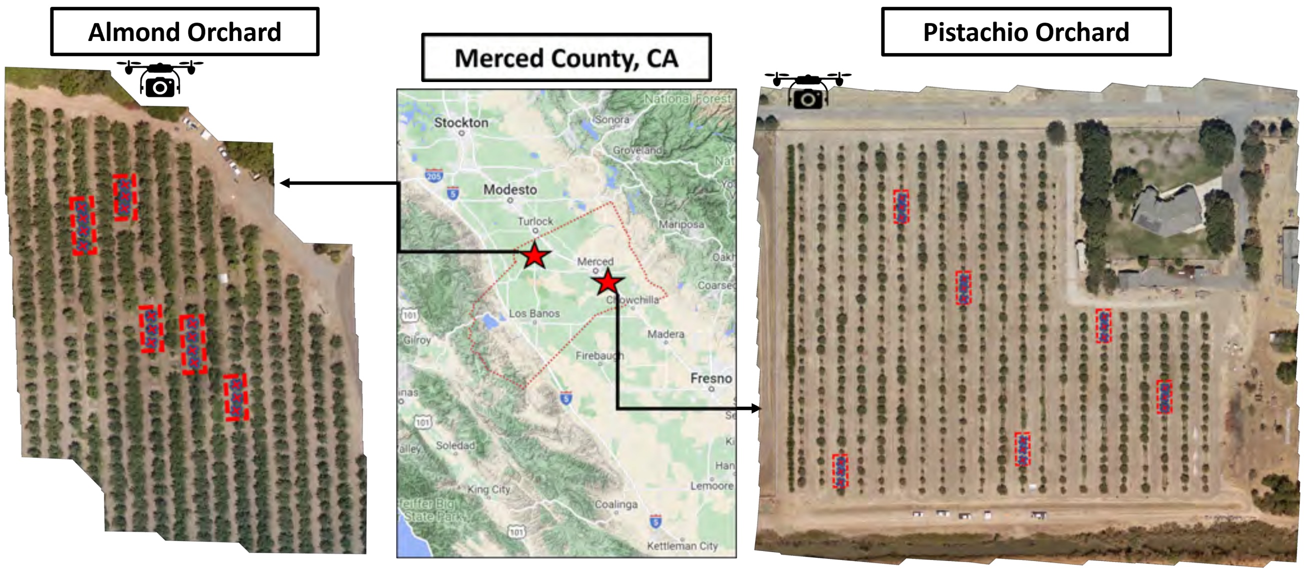

FIGURE 2: Test sites located in Merced, California. A total of 18 pistachio trees and 17 almond trees were considered for the experiments. The location of trees under assessment are shown using red markers and bounding boxes.

2.2 Ground Measurements

Throughout each day of experiment, stem water potential (SWP) measurements were collected within 1-2 hours of solar noon, approximately around 1 PM. To account for variability in SWP measurements within target trees, three leaves from the lower shaded canopy of each sample tree were chosen for SWP measurements. The resultant data was averaged to produce a mean SWP value per tree for subsequent analysis. These measurements were performed using the PMS-615 pressure chamber (PMS Instrument Company, Albany, OR, USA). Prior to being detached from the tree and analyzed in the pressure chamber, the leaves were sealed in aluminum bags for a minimum duration of 15 minutes. Encasing the leaves in bags before conducting the SWP measurements is crucial for obtaining precise results. This procedure guides the leaf toward an equilibrium state and mitigates discrepancies that could arise from continuous photosynthesis and transpiration within the leaves (Lampinen et al., 2015).

Concurrently with the collection of SWP measurements (±1 hour of solar noon), leaf temperature was recorded from three distinct leaves located at three different sides of each tree on the lower canopy. The recorded measurements were subsequently averaged to represent the canopy temperature T_c for each sample tree. The leaf temperature data was measured using a TM0866 non-contact infrared thermometer (PerfectPrime, Barbican, UK) with $0.1°C$ resolution and ±1% accuracy. Each temperature measurement was conducted at a 5-10cm distance from the leaf center and perpendicular to its surface.

2.3 Aerial Imaging

Flights were conducted within an hour of the solar noon, which occurred approximately at 1 pm local time, to minimize issues related to canopy shading. Aerial imaging is performed using DJI P4 multispectral agricultural drone (SZ DJI Technology Co., Ltd., Shenzhen, China) equipped with RTK-GNSS system for precise georeferencing. The built-in imaging system is composed of an RGB camera and a five-band multispectral camera array, all of which are mounted on a 3-axis stabilized gimbal. The multispectral array encompasses five distinct bands: blue (B: 450 nm ± 16 nm), green (G: 560 nm ± 16 nm), red (R: 650 nm ± 16 nm), red edge (RE: 730 nm ± 16 nm), and near-infrared (NIR: 840 nm ± 26 nm). Each band was captured by a dedicated 2 MP camera with a global shutter.

During each flight mission, images were captured from an altitude of approximately 100 meters above the ground providing $4cm/pixel$ resolution. Additionally, the integrated upward looking sunlight sensor records solar irradiance during the flight, which allows for instantaneous referencing of spectral reflectance. The collected spectral data were processed through the computer software DJI Terra version 3.7.0 to create orthomosaic maps for each orchard. The DJI Terra software was utilized for radiometric correction to produce one color composite along with five indexed maps for specific vegetation parameters: Normalized Difference Vegetation Index (NDVI), Green Normalized Difference Vegetation Index (GNDVI), Optimized Soil-Adjusted Vegetation Index (OSAVI), Leaf Chlorophyll Index (LCI), and Normalized Difference Red Edge (NDRE). The spectral indices were calculated as follows: NDVI was computed as $(R_{nir} - R_{red})/(R_{nir} + R_{red})$, GNDVI as $(R_{nir} - R_{green})/(R_{nir} + R_{green})$, OSAVI as $(R_{nir} - R_{red})/(R_{nir} + R_{red} + 0.16)$, LCI as $(R_{nir} - R_{rededge})/(R_{nir} + R_{red})$, and NDRE as $(R_{nir} - R_{rededge})/(R_{nir} + R_{rededge})$. We utilized the Computer Vision Annotation Tool (CVAT) to manually extract the location of selected canopies from the orthomosaic maps. NDVI maps were utilized for annotation due to their enhanced clarity in identifying canopy boundaries. With the aid of these annotated NDVI maps, precise locations of the target tree canopies were determined. Subsequently, these geolocations were leveraged to automate the extraction of index values from all the other maps. Image processing and all subsequent analysis were carried out using Python. Upon extraction of the index values from each tree canopy, the median of all values was used to represent the corresponding vegetation index for each sample tree.

2.4 Weather Sensors

Local weather stations were installed in both orchards to collect the ambient temperature, barometric pressure, and relative humidity. These weather data were collected every ten minutes during the 2022 growing season. The availability of a wireless network in the PO allowed for real-time monitoring and cloud storage of the data. In contrast, the lack of a reliable internet network in the AO prevented us from transferring data to an internet-connected cloud server. Therefore local data storage was adopted in this area. Weather stations include a BME688 sensor (Bosch Sensortec, Kusterdingen, Germany) and an ESP8266 chip (Espressif Systems, Shanghai, China) with IEEE 802.11 b/g/n Wi-Fi and built-in TCP/IP networking software. The BME688 sensor measures temperature, humidity, pressure, and gas resistance, providing a comprehensive environmental data. The ESP8266 chip enables wireless connectivity and allows the weather stations to transmit data to a central server for real-time monitoring and analysis. In the PO, two ordinary D size 1.5 V batteries connected in series could provide the required energy to each weather station. The weather station in AO relied on solar cells as a sustainable energy source.

2.5 Feature Selection

Initially, we considered a total of 15 features for the prediction of SWP in both PO and AO. Out of these, nine were derived from weather features, representing minimum, maximum, and mean values of air temperature $T(°C)$, air pressure $P(hPa)$, and relative humidity $RH(\%)$ calculated for each day of the experiment. The remaining features included five vegetation indices, NDVI, GNDVI, OSAVI, LCI, NDRE, and a thermal feature T_c representing the canopy temperature, which are all calculated individually for each sample tree.

TABLE 1: Final selection of input variables used in machine learning models to predict stem water potential.

	Selected Input Features						**Output**
Pistachio	T_{mean}	P_{min}	RH_{min}	T_c	$OSAVI$	$NDRE$	SWP (ψ)
Almond	T_{max}	P_{min}	RH_{min}	T_c	$NDVI$	$NDRE$	SWP (ψ)
Unit	$[°C]$	$[hPa]$	$[\%]$	$[°C]$	–	–	$[bar]$
Input type	weather	weather	weather	thermal	Multispectral (MS)	Multispectral (MS)	

The correlation heatmaps based on the Pearson method were generated and are illustrated in Figure 3. Before deploying machine learning models for SWP prediction, inputs were filtered and checked for potential multicollinearity. For each weather feature (T,P,RH) represented by minimum, mean, and maximum values on each day of experiment, we selected the one with highest correlation with the SWP. This choice was made to avoid redundancy in inclusion of weather features. As a result one representative weather feature was chosen from each group, resulting in $(T_{mean}, P_{min}, RH_{min})$ for PO, and $(T_{max}, P_{min}, RH_{min})$ for AO, as seen in table 1. Then, a cutoff value of 0.75 was applied to remove features that are highly correlated with other features. This means that one out of the two features with absolute correlation coefficients greater than $|r| > 0.75$, was subsequently excluded from the analysis. Among those two features, the one with lower correlation with SWP is eliminated. From Figure 3 it can be observed that in both crops, T_c was not highly collinear with any other feature. Additionally in PO, NDVI and GNDVI with OSAVI, and LCI with NDRE were highly correlated thus eliminated from the input features. In AO, GNDVI and OSAVI with NDVI, and LCI with NDRE were highly correlated thus eliminated from the input features. Filtering the features based on correlation coefficients led to the establishment of a final collection of predictors. Consequently, six input features, as demonstrated in table 1, were selected to be used for SWP prediction in PO and AO using machine learning. These features were $T_{mean}, P_{min}, RH_{min}$, T_c, $OSAVI$, $NDRE$ for PO, and $T_{max}, P_{min}, RH_{min}$, T_c, $NDVI$, $NDRE$ for AO.

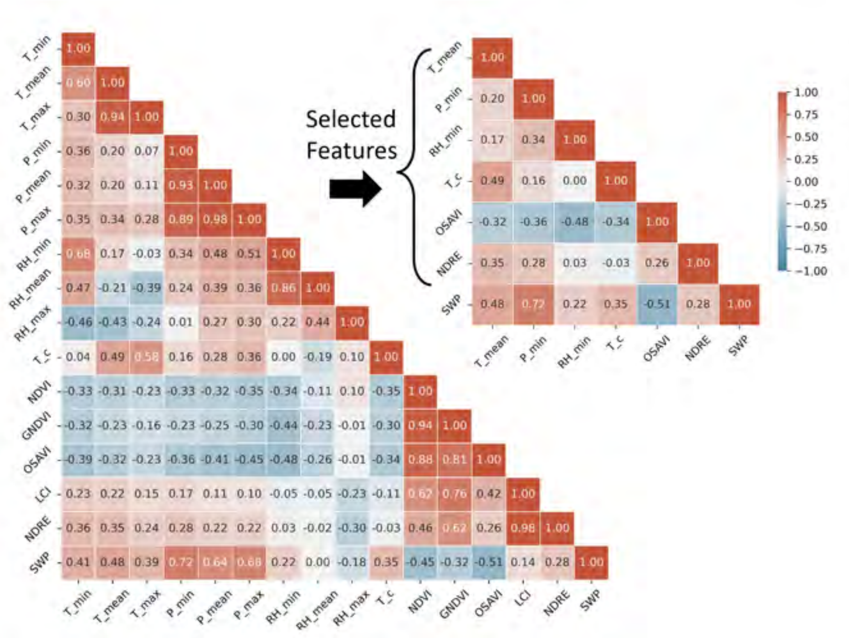

(a) PO correlation heatmaps

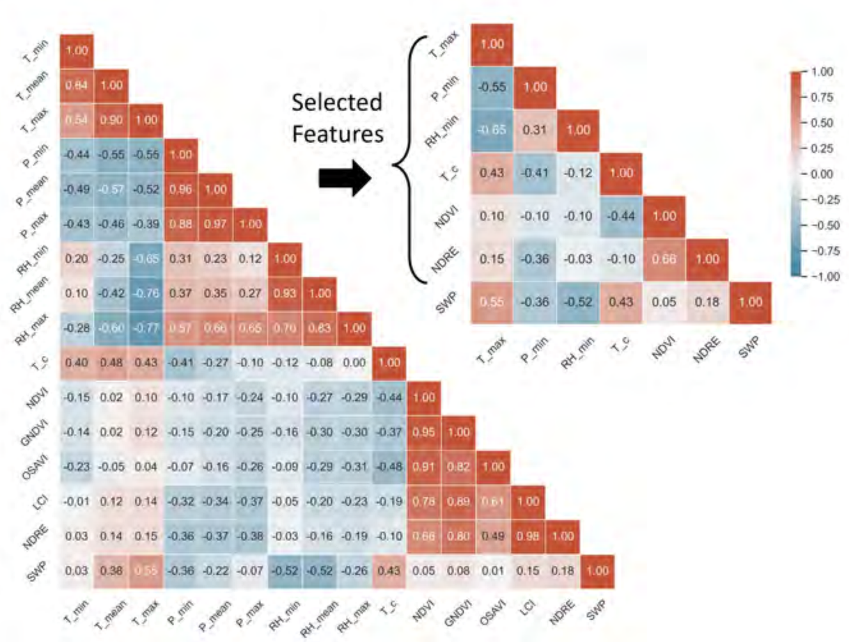

(b) AO correlation heatmaps

FIGURE 3: Pearson correlation heatmaps for (a) Pistachio (PO) and (b) Almond orchard (AO). (left) represents the Pearson correlation heatmap with all 15 inputs (right) filtered Pearson correlation heatmap with 6 inputs that were used in ML models for SWP prediction. T, P, RH refer to weather temperature, pressure, and relative humidity reflecting minimum, mean, and maximum values measured on each day of experiment. T_c is the canopy temperature, NDVI, GNDVI, OSAVI, LCI, NDRE are vegetation indices (VIs), which are measured for each tree individually throughout the season.

2.6 Machine Learning Models

We used six machine learning (ML) models, including Random Forest (RF), Support Vector Machine (SVM), Gaussian Naive Bayes (GNB), Decision Tree (DT), K-Nearest Neighbors (KNN), and Artificial Neural Network (ANN). These models were implemented using the Scikit-learn (Pedregosa et al., 2011), an open-source machine learning library developed for Python.

DT and RF possess distinct characteristics in handling classification and regression problems. DT functions by systematically dividing data into progressively smaller subsets. In the constructed tree-like diagram, every node symbolizes a comparison based on a specific feature, whereas the terminal leaves signify the final decision or prediction. RF stands as a prime example of ensemble learning, where the power of multiple decision trees is harnessed to form an aggregated predictive model. Ensemble learning methods aim to boost predictive performance by creating a composite model from a collection of simpler base models, each reflecting a unique hypothesis. This approach allows for integrating diverse hypotheses, often yield superior predictive results. RF offers robustness against noise and is less prone to overfitting thanks to the averaged predictions across multiple trees (Liakos et al., 2018; Quinlan, 1993). GNB belongs to the family of Bayesian models, which are probabilistic graphical models employed within the framework of Bayesian inference. This supervised learning model is applicable to both classification and regression problems. Despite its naive assumption of feature independence, the computational efficiency of GNB makes it an ideal choice for tasks necessitating quick and real-time predictions (Rish et al., 2001; Liakos et al., 2018). SVMs are key tools in ML, renowned for their adaptability in handling regression and classification tasks as well as clustering. They function by constructing a maximum margin hyperplane in a high-dimensional space, distinguishing between various classes while maximizing the margin between nearest points or support vectors (Chang and Lin, 2011). KNN is a supervised learning algorithm that works without any inherent assumptions about the underlying dataset. It is widely used for classification where it assigns classes to new data points based on their proximity to existing labeled examples. The k in KNN represents the number of nearest neighbors the algorithm considers when making its prediction. Choosing an optimal k value is the key to its effectiveness and performance(Taunk et al., 2019; Ray, 2019). ANN is a computational model inspired by the biological neural networks, which offers a distinctive approach to handle intricate and highly non-linear problems. A specific type of ANN is the Multi-Layer Perceptron (MLP), which functions as a feed-forward network. The neurons in each layer are interconnected to the neurons of the subsequent layer through weighted connections. During the learning phase, these weights are adjusted using techniques such as backpropagation (Messikh et al., 2017; Delashmit et al., 2005). In this study, we used MLP for ANN analysis to map the complex relationships between the input data and the output predictions.

2.7 Model Evaluation

To evaluate the predictive capabilities of the machine learning algorithms, we partitioned the datasets from each orchard such that 75% was allocated for the training and validation of the models, while the remaining 25% was set aside for testing their performance. The test dataset was completely isolated from the training/validation dataset to avoid overfitting and data leakage. The dataset was then subjected to a standard scaling process, where each feature in the training set was scaled to have a mean of zero and a standard deviation of one. This step prevents features with larger values from dominating others during the training process, ensuring that each feature contributes proportionately to the final prediction. Next, each classifier was optimized to provide the highest performing predictive model, a strategy known as hyperparameter optimization. For the optimization process, we utilized a randomized search among the hyperparameters along with a 10-fold stratified cross-validation (CV) within the training dataset. This method partitions the original sample into ten equal-sized subsamples. In our study, the use of stratified CV was essential due to the imbalanced nature of the classes. This technique allows each fold to represent the overall class distribution accurately, thus preventing the model from being biased toward the majority class. This enhances the robustness and generalization of the model as it accounts for the scarcity of minority class instances. Of the ten subsamples, one is retained as validation set and the remaining are used as training data. The cross-validation process is then repeated ten times, with each of the ten subsamples used once as validation data. The optimal set of hyperparameters was eventually determined based on the best average performance across all folds. Through the optimization process, it is ensured that the trained models are not exposed to the final test dataset to prevent data leakage and overfitting.

The optimized classifiers were subsequently utilized to evaluate the performance of test datasets. We used accuracy, F1-score, and Area Under Curve (AUC) of the Receiver Operating Characteristic (ROC) as metrics to assess the performance of each classifier. Accuracy is defined as the proportion of correct predictions relative to the total number of predictions. Consider class 0 as negative and class 1 as positive. The F1-score is first calculated on a per-class basis and defined as the harmonic mean of the precision and recall. Within each class, precision is the number of true positives (TP) or correctly identified positive instances by the model in the positive class, divided by all positively identified instances ($TP+FP$) (whether correct or incorrect), with FP denoting false positives. Recall is the number of true positives TP divided by all samples that should have been identified as positive $TP+FN$, where FN represents false negatives. As a result, the average of F1-scores calculated for each class are reported. The ROC curve is created by plotting the true positive rate (TPR) against the false positive rate (FPR) at various thresholds. The AUC is then computed by integrating the area under ROC curve. AUC provides a single scalar value representing the expected performance of the classifier. An AUC score close to 1 implies that the model has excellent ability to distinguish between classes, while an AUC score close to 0.5 indicates that the model is not classifying groups better than random classification. The regression model was similarly trained using a 10-fold CV and its performance was evaluated using the coefficient of determination R^2, root mean square error $RMSE$, and mean absolute error MAE.

2.8 Data splitting

Tentative categories based on SWP values have been defined by the University of California Agricultural Extension (UCANR) for different type of crops. For instance, pistachio trees are considered non-stressed at -9 to -12 bars, moderately stressed at -12 to -14 bars, and severely stressed at values less than -15 bars. Almond trees are categorized as experiencing minimal stress at -6 to -10 bars, mild stress at -10 to -14 bars, moderate stress at -14 to -18 bars, high stress at -18 to -22 bars, and severe stress at values below -30 bars (Savchik et al., 2024).

For ML classification and given the total number of collected SWP readings and their distribution across these categories, we adopted a binary classification approach. This decision was primarily driven by the overall water levels observed in the experimental orchards and the specific conditions of the sampled trees. Upon examination of the SWP readings from the almond orchard (AO), we noted a significant level of water stress, with approximately 74% of the total SWP readings falling below -18 bars. Conversely, the pistachio trees in the corresponding orchard were observed to be well watered, with about 70% of the SWP readings exceeding -9 bars. To effectively categorize the orchards based on water levels, we defined thresholds for binary classification. In PO, a cutoff SWP value of -9 bars and in AO a cutoff of -18 bars were applied to separate trees with different stress levels. As illustrated in Figure 4, the total number of observations for the pistachio was $n = 126$, whereas for the almond, it was 119. Some incomplete data points within the almond dataset were identified and subsequently excluded from the analysis to get a total number of $n = 111$ observations in AO. As a result, 25% of the data in each orchard was used for testing and the remaining 75% was considered for training and validation of the ML models.

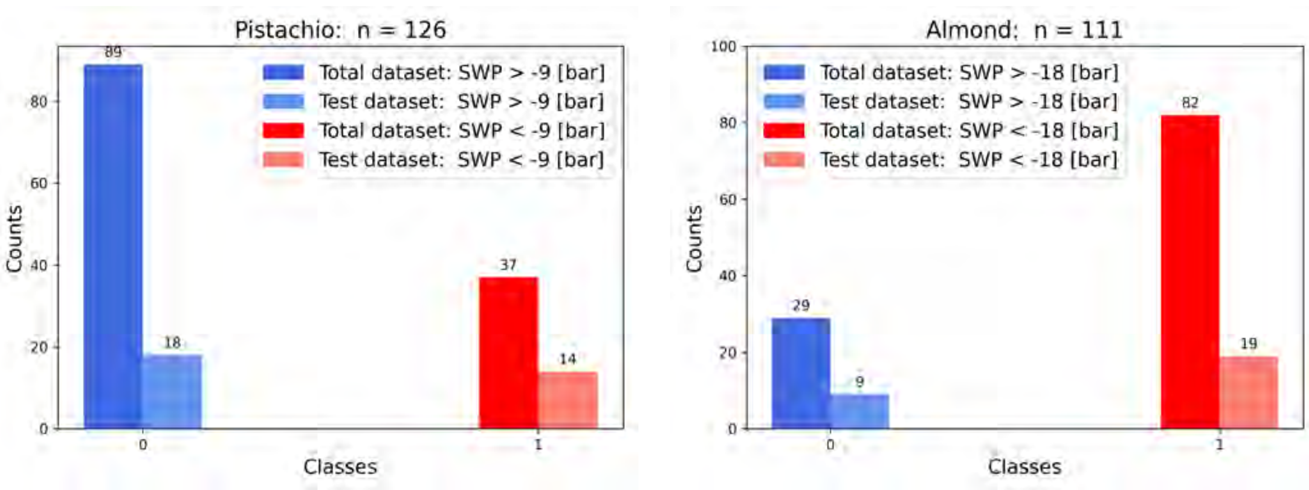

(a) PO (b) AO

FIGURE 4: Binary classes of collected stem water potential (SWP) data where 25% of the total dataset is set aside as test set to evaluate the performance of ML models. n denotes the total number of dataset in (a) the pistachio orchard with $n = 126$ and (b) the almond orchard with $n = 111$.

3 RESULTS AND DISCUSSIONS

3.1 Collected Data

Weather and MS data along with T_c and SWP (ψ), were recorded for PO and AO, during the 2022 growing season. SWP values for each DOY are illustrated in Figure 5. Among the seven days of experiment in PO, the lowest mean $|\psi|$ value was $|\psi| = 5.4$ $bars$ with standard deviation of $\sigma = \pm1.31$ $bars$, observed on DOY 172, which corresponds to the second day of experiment. Conversely, the highest mean $|\psi|$ value was $|\psi| = 10.8$ $bars$ with $\sigma = \pm2.17$ $bars$, observed on DOY 224, which corresponds to the last day of experiment. The standard deviations were ranged between $0.91 < |\sigma| < 2.17$ in PO. Among the seven days of experiment in AO, the lowest mean $|\psi|$ value was $|\psi| = 14.3$ $bars$ with standard deviation of $\sigma = \pm1.67$ $bars$, observed on DOY 211, which corresponds to the fifth day of experiment. Conversely, the highest mean $|\psi|$ value was $|\psi| = 26.1$ $bars$ with $\sigma = \pm2.96$ $bars$, observed on DOY 215, which corresponds to the sixth experiment. The standard deviations were ranged between $1.67 < |\sigma| < 4.37$ in AO. Considering all collected SWP data during the season, PO had a mean of $|\overline{\psi}| = 8.0 \pm 2.41$ $bars$ and AO had a mean of $|\overline{\psi}| = 21.0 \pm 4.70$ $bars$.

Weather data were continuously monitored through local weather stations installed in both orchards for which the results are demonstrated in Figure 6. As shown in table 1, the final selection of weather features were $T_{mean}, P_{min}, RH_{min}$ for PO, and $T_{max}, P_{min}, RH_{min}$ for AO. During the seven days of experiment in PO, the lowest

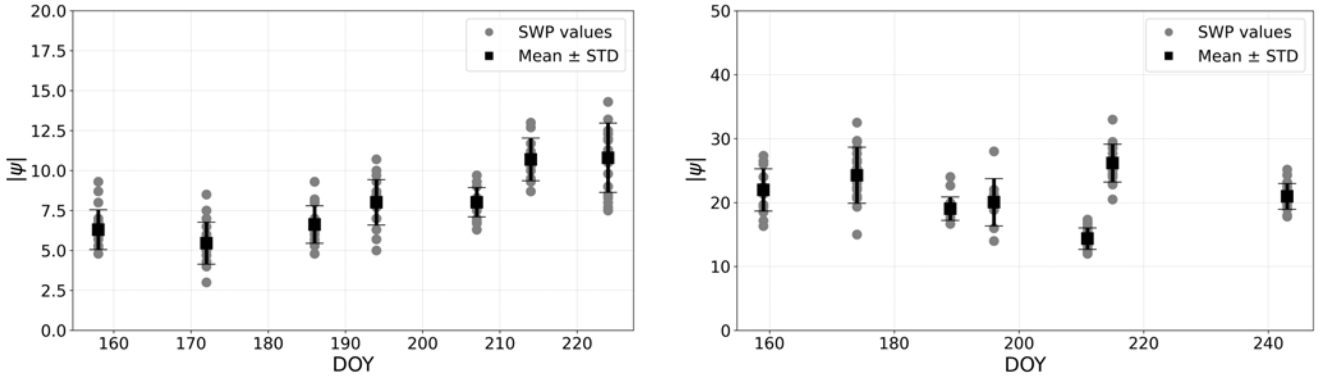

(a) PO (b) AO

FIGURE 5: Collected stem water potentials (ψ) during the 2022 season versus the corresponding day of year (DOY) for the (a) pistachio orchard (b) almond orchard.

and highest average temperature T_{mean} were 25.5°C and 31.4°C representing the first (DOY 158) and sixth (DOY 214) experiments. The first and the third days of experiment corresponding with DOY 158 and 178 recorded the lowest and highest RH_{min} at 13.8% and 31.4%, respectively. The lowest and highest P_{min} were respectively observed on DOY 172 and 224 at 1002.4 hPa and 1006.0 hPa, which represent the second and the seventh days of experiment. During the seven days of experiment in AO, the lowest and highest average temperature T_{max} were 34.9°C and 41.4°C representing the fifth (DOY 211) and second (DOY 174) experiments. The second and the fifth days of experiment corresponding with DOY 174 and 211 recorded the lowest and highest RH_{min} at 23.2% and 48.3%, respectively. The lowest and highest P_{min} were respectively observed on DOY 174 and 189 at 1005.8 hPa and 1011.6 hPa, which represent the second and the third days of experiment. Considering the Pearson correlation coefficients among the weather features as seen in Figure 3, P_{min} ($r = 0.72$) in pistachio and T_{max} ($r = 0.55$) in almond had the highest linear correlation with SWP. The correlations $r = 0.48$ and $r = 0.22$ were respectively observed for T_{mean} and RH_{min} in PO, and $r = -0.52$ and $r = -0.36$ for P_{min} and RH_{min} in AO.

The selected thermal and MS input features, as demonstrated in table 1, were T_c, $OSAVI$, $NDRE$ for PO, and T_c, $NDVI$, $NDRE$ for AO. These features were plotted against absolute SWP ($|\psi|$) and the results along with their best fitted regression lines are demonstrated in Figure 7. In PO and AO, the correlations between T_c and SWP were $r = 0.35$ and $r = 0.43$, respectively. Among the VIs, OSAVI in pistachio with $r = -0.51$ and NDRE with $r = 0.18$ in almond exhibited higher linear relationships with SWP. NDRE in PO with $r = 0.28$ and NDVI in AO with $r = 0.05$ had the weakest linear relationship with SWP among the selected thermal and MS features. In PO the trees had higher water levels while in AO the trees were mostly under water stress. This signifies that MS indices were more sensitive to SWP in the well-watered PO. Conversely, MS indices demonstrated lower sensitivity to SWP in the water stressed AO while T_C was more sensitive to the changes in SWP. In PO, OSAVI had the highest coefficient of determination with SWP at $R^2 = 0.26$ while in AO, $R^2 = 0.19$ was highest between T_c and SWP.

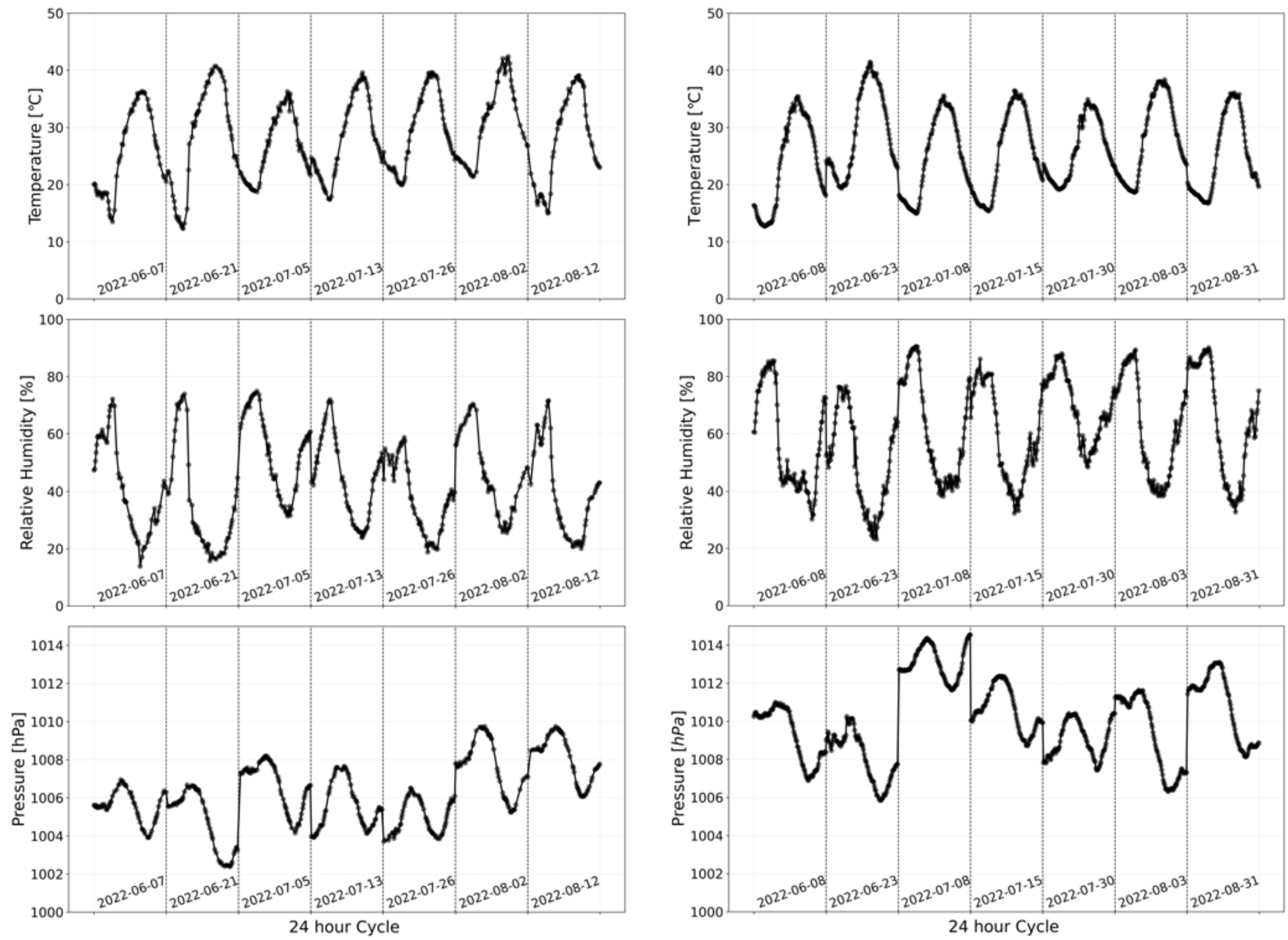

(a) PO

(b) AO

FIGURE 6: Collected weather data during each day of experiment in (a) pistachio (PO) and (b) almond orchard (AO). Each weather data is illustrated for 24h cycles starting at midnight 00:00 (12am).

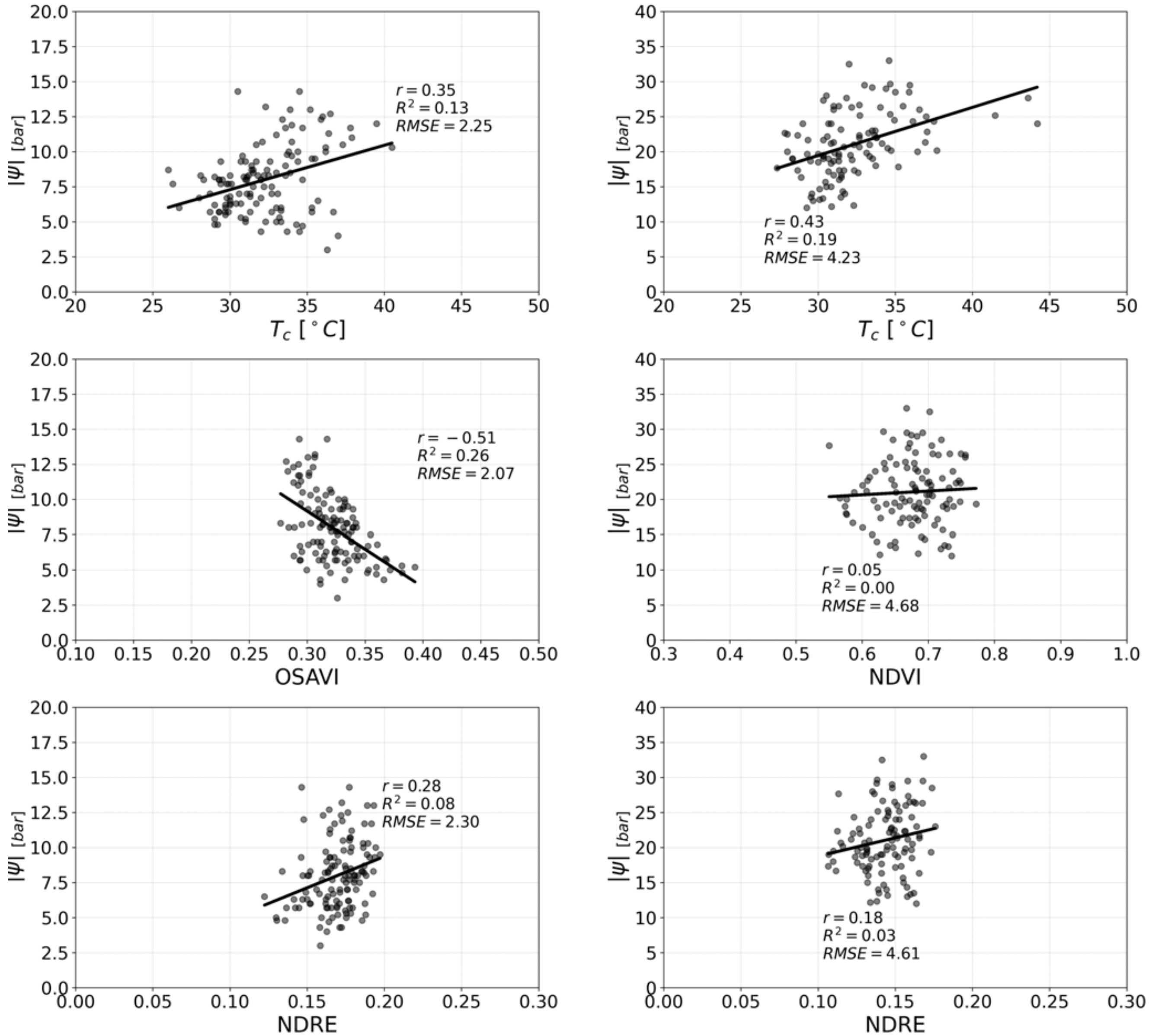

(a) PO

(b) AO

FIGURE 7: Selected thermal and multispectral (MS) features throughout the season versus absolute SWP ($|\psi|$) values in (a) pistachio orchard and (b) almond orchard. T_c represents the canopy temperature and OSAVI, NDVI, and NDRE represent the MS vegetation indices.

3.2 Classification using Machine Learning

The resulting optimized classifiers were subsequently deployed to predict the test dataset. Figure 8 illustrates the classification performance of the implemented machine learning models predicting SWP values in both the PO and AO. For each model, the classification accuracy of the test dataset along with their performance across each fold of cross-validation during the training phase are elucidated. The accuracy of each classifier was obtained based on the ratio of correct predictions to the total number of predictions made by the model. All models provided accuracies higher than 79%. For the PO, the Random Forest (RF) and Decision Tree (DT) models delivered superior performance, each achieving an accuracy rate of 88%. In the AO, RF shared the highest accuracy rate of 89% with Support Vector Machine (SVM), K-nearest neighbors (KNN), and Artificial Neural Network (ANN) models.

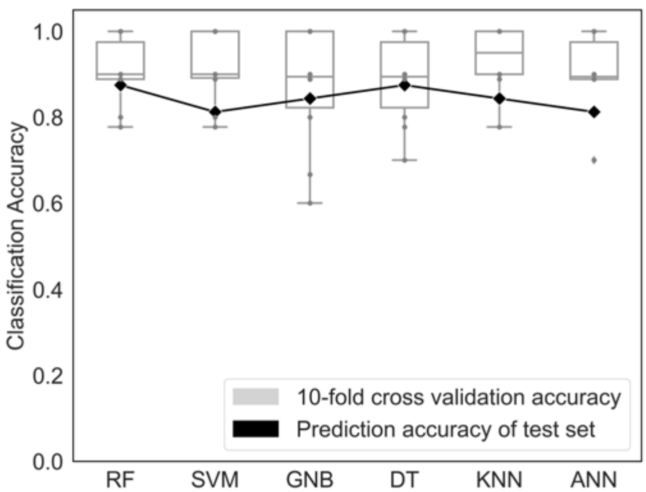

(a) PO

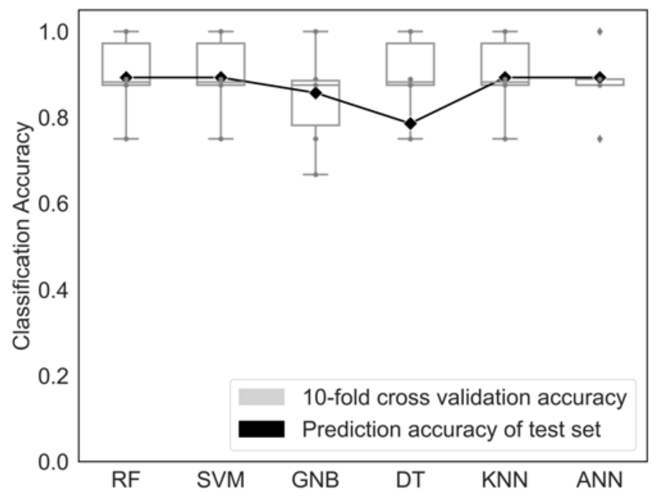

(b) AO

FIGURE 8: Performance of ML classifiers namely Random Forest (RF), Support Vector Machine (SVM), Gaussian Naive Bayes (GNB), Decision Tree (DT), K-Nearest Neighbors (KNN), and Artificial Neural Network (ANN) predicting SWP in pistachio (PO) and almond orchard (AO). The gray patch represents the accuracy of each fold during the cross-validation phase and the black patch shows the prediction accuracy of the best trained model on the test set.

Table 2 further elucidate the performance of each classifier, detailing additional metrics, including Cross-Validation (CV) averages, F1-scores, and Area Under Curve (AUC) values. It is noteworthy that the classifiers also demonstrated consistent performance across the folds during the CV phase. In PO, the mean of CV values were ranged between 87-94% whereas in AO this values were ranged between 86-89%. With an exception to the F1-score of DT in AO, which was 75%, F1-scores in both PO and AO were ranged between 81-87%. The F1-score acts as a measure of a model's performance in correctly identifying instances in each class. The F1-score takes into account both precision and recall, providing a more comprehensive picture of model performance across all classes. This is particularly critical when dealing with datasets with imbalanced class distributions, as it provides a more nuanced understanding of a model's performance than accuracy alone. Moreover, the AUC which is calculated from the ROC curve, provides further insights into the model's ability to distinguish between the classes at various thresholds. An AUC score of 0.5 represents a model with no discrimination capacity, effectively performing no better than random chance. On the other hand, an AUC of 1.0 (100%) signifies perfect classification. High values of AUC imply that the model is making correct classifications while avoiding misclassifications. In the PO, the F1-scores of the applied ML classifiers varied from 81% (ANN and SVM) to 87% (RF and DT). Meanwhile, the AUC values ranged from 82% (KNN) to 88% (GNB) underlying a satisfactory ability while distinguishing between the classes. In the AO, the F1-scores ranged from 75% to 86%. The lowest AUC value was 77% by DT and the highest values was achieved by SVM and ANN at 93%. Overall, these metrics represent relative reliability of the ML models employed for SWP prediction in this study.

TABLE 2: Quantitative analysis on the performance of ML classifiers predicting SWP in the pistachio (PO) and almond orchard (AO).

		PO				AO			
Models	**Input**	**Accuracy**	**$\overline{\text{CV}}$**	**F1-score**	**AUC**	**Accuracy**	**$\overline{\text{CV}}$**	**F1-score**	**AUC**
RF	All	0.88	0.91	0.87	0.86	0.89	0.89	0.86	0.88
SVM	All	0.81	0.92	0.81	0.87	0.89	0.89	0.86	0.93
GNB	All	0.84	0.87	0.84	0.88	0.86	0.86	0.82	0.87
DT	All	0.88	0.89	0.87	0.86	0.79	0.89	0.75	0.77
KNN	All	0.84	0.94	0.84	0.82	0.89	0.89	0.86	0.86
ANN	All	0.81	0.91	0.81	0.83	0.89	0.88	0.86	0.93

Confusion matrices were demonstrated in the Figure 9. The total number of test datasets in PO was $n_{test} = 32$ and in AO was $n_{test} = 28$ representing 25% of total dataset in each orchard. The RF and DT were the best classifiers in PO providing 28 correct and 4 wrong predictions. There were 17 TN and 11 TP as well as 1 FP and 3 FN in both RF and DT. This also reflects better prediction accuracy towards the majority class or class 0, in PO. Conversely, SVM and ANN had the lowest accuracies with 26 correct and 6 wrong predictions reflecting 16 TN, 10 TP, 2 FP and 4 FN in SVM, and 15 TN, 11 TP, 3 FP and 3 FN in ANN. In AO, RF, DT, SVM, and ANN were the best classifiers providing 25 correct and 3 wrong predictions. In all of these classifiers, there were 6 TN and 19 TP as well as 3 FP and 0 FN. This also reflects better prediction accuracy towards the majority class or class 1 in AO. Conversely, DT had the lowest accuracy with 22 correct and 6 wrong predictions reflecting 6 TN, 16 TP, 3 FP and 3 FN.

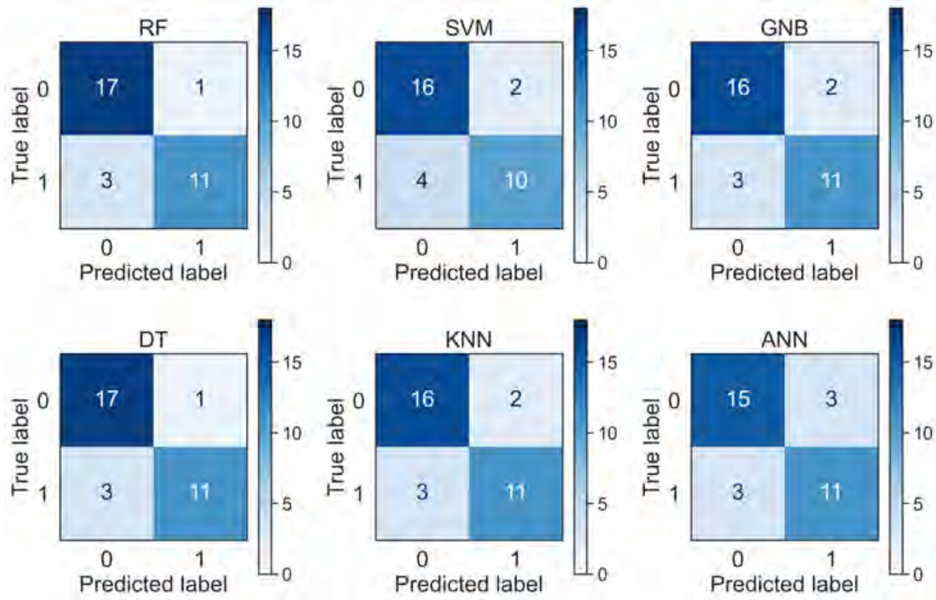

(a) PO

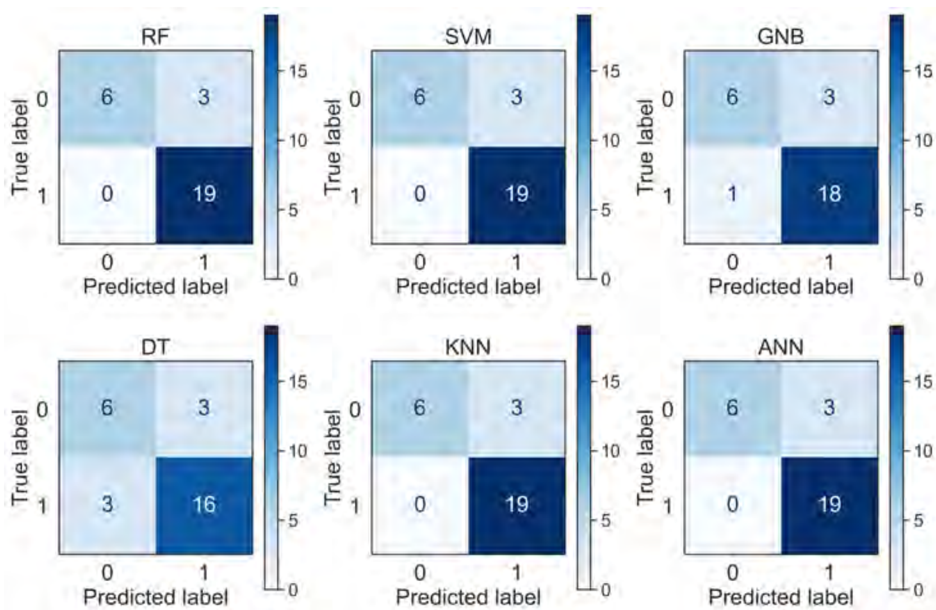

(b) AO

FIGURE 9: Confusion matrices representing the results of ML classifiers predicting SWP in (a) pistachio orchard (b) almond orchard.

RF provided high accuracy and more consistency classifying SWPs in both orchards. RF has been extensively explored and employed in numerous studies due to its high tolerance for outliers and noise, along with its resistance to overfitting (Fan et al., 2021; Benos et al., 2021; Pagano et al., 2023). An additional advantage of RF is its capacity to calculate feature importance percentages. Feature importance in RF provides a measure of the contribution each feature makes to the predictive power of the model. This is calculated using a combination of the mean decrease accuracy (MDA) and mean decrease Gini (MDG) metrics, allowing for a comprehensive understanding of the relevance of each feature. This characteristic can be particularly useful in understanding and interpreting the model's decisions (Virnodkar et al., 2020). In the context of our study, the feature importance results offered by the RF model can illuminate the relative contribution of each feature to the SWP prediction. Such understanding is instrumental in formulating data acquisition strategies for subsequent research studies related to tree water status assessment. Figure 10 demonstrates the importance of features used to determine SWP in almond and pistachio trees. Weather features contributed the highest to the SWP prediction. In the PO, the feature with the greatest influence was P_{min}, accounting for 30% of feature importance. In the AO, T_{max} was the most critical feature, with a contribution of 36%. The T_{max} and RH_{min} collectively dominated nearly 68% of the decisions made by the RF model in the AO. In both PO and AO, T_c demonstrated a higher importance relative to individual MS VIs. It accounted for approximately 22% of the importance in PO and 10% in the AO. In terms of MS VIs, OSAVI (20%) in PO and NDVI (7.5%) in AO showed higher importance than NDRE in both crops. However, the disparity was more noticeable between OSAVI and NDRE in PO, which was about 10% compared to the minimal difference between NDVI and NDRE in AO at about 2-3%. The overall contribution of weather, thermal, and MS features to SWP classification in PO were, 48%, 22%, 30%. The overall contribution of weather, thermal, and MS features to SWP classification in AO were, 77%, 10%, 13%.

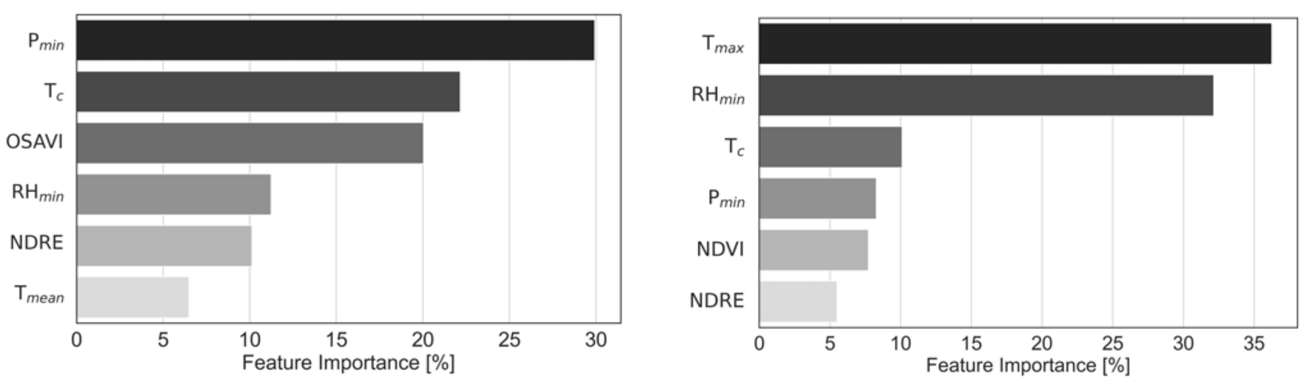

(a) PO

(b) AO

FIGURE 10: Feature importance provided by the Random Forest (RF) classifier for (a) pistachio orchard and (b) almond orchard.

Given the observations in this study, the AO was under considerable water stress, with nearly 74% of the SWP values registering below -18 bars. This is indicative of high stress and notable water deficiency in the almond trees (see Figure 4). In contrast, the PO demonstrated an entirely different watering profile with a predominantly hydrated state. About 70% of the SWP measurements were above -9 bars, highlighting an excessive hydration status for the pistachio trees. The difference in hydration profiles of the two orchards brings into focus the role of atmospheric features in SWP determination as seen in Figure 10. Given the distinct differences in water stress levels between the two orchards, it appears that the importance of these atmospheric variables in SWP prediction fluctuates in accordance with the level of tree water status. Particularly, under conditions of high water stress, as observed in the almond orchard, atmospheric parameters like air temperature and air pressure may gain prominence towards the determination of SWP.

Environmental factors such as micro-climate, soil variation, and root system differences significantly impact tree water status within an orchard. Micro-climate fluctuations influence water uptake, while soil properties affect moisture availability to roots. Understanding root system diversity is crucial. For precise irrigation, knowledge about spatial water variability and micro-climate are essential (Peters et al., 2010; Ntshidi et al., 2023). Given the complex interaction of various environmental factors within an orchard, atmospheric measures alone might not offer a comprehensive picture of tree water needs. While these parameters play a pivotal role in estimating the overall tree water status in an orchard, they are not able to determine the water status of an orchard on a per-tree basis. For a more precise prediction of SWP on a tree-by-tree basis, more individualized features may be required. Among these exclusive features, CWSI(T_c,T_a, VPD) holds a distinct importance. In other studies, CWSI has also been found to have a good correlation with SWP both in pistachios (Jafarbiglu and Pourreza, 2022; Gonzalez-Dugo et al., 2015; Testi et al., 2008) and almonds (Gonzalez-Dugo et al., 2012; García-Tejero et al., 2012). This can be attributed to the heightened sensitivity of canopy temperature T_c to fluctuations in plant water stress. T_c is capable of identifying subtle changes in plant water status that other multispectral VIs often overlook. Its high sensitivity renders it a potentially powerful tool for monitoring plant water status and predicting SWP values at a tree-specific level. The ability to reconcile distinct but interconnected sources of information would be key to developing robust machine learning models for accurate and reliable prediction of SWP values.

3.3 Classification and Regression using RF

The RF classification and regression models were used to predict SWP with different input features, shown in table 3. For PO with all inputs, the RF model demonstrated strong classification performance, achieving an accuracy of 88%, an average 10-fold cross-validation ($\overline{CV}$) score of 91%, a F1-score of 0.87, and an AUC of 0.86. The regression metrics were also satisfactory with R^2 value of 0.70, RMSE of 1.13, and MAE of 0.84, indicating good predictions. When the model inputs were limited to MS and thermal features only, the classification accuracy reduced to 78%, the $\overline{CV}$ score to 84%, F1-score to 0.72, and AUC to 0.78 along with noticeable declines in regression outcomes (R^2 of 0.46, RMSE of 1.54, and MAE of 1.29). A further reduction to only MS features led to further decreases in both classification and regression metrics, with classification accuracy dropping to 72%, $\overline{CV}$ to 83%, F1-score to 0.68, AUC to 0.73, as well as R^2 of 0.33, RMSE of 1.72, and MAE of 1.38. These results underscore the challenges in achieving high predictive accuracy for SWP with only MS used as input feature.

Similar trends were observed in AO although the effect of reduced features on model performance were higher. Utilizing all inputs, the RF model showed good classification accuracy at 89%, with a $\overline{CV}$ score of 89%, F1-score of 0.86, and AUC of 0.88. The regression metrics were less robust than in PO with R^2 of 0.55, RMSE of 3.18, and MAE of 2.44. However, restricting the inputs to MS and thermal data significantly reduced the model performance and resulted in a stark decrease in all metrics including accuracy to 61%, $\overline{CV}$ to 76%, F1-score to

0.51, AUC to 0.51, as well as R^2 to 0.26 while RMSE and MAE increased to 4.11 and 3.15, respectively. While the classification reached an accuracy of 61% the low AUC score of 0.51 highlights the classifier's inability in classification and distinguishing between classes. Using MS features as input, the RF regression and classification models performed poorly thus the results are not included in the analysis.

TABLE 3: Using the Random Forest (RF) model for comparison between various inputs. The units for RMSE and MAE are $bars$.

			Classification				Regression		
Model	**Orchard**	**Input**	**Accuracy**	$\overline{\textbf{CV}}$	**F1-score**	**AUC**	R^2	**RMSE**	**MAE**
RF	PO	All	0.88	0.91	0.87	0.86	0.70	1.13	0.84
RF	PO	MS, Thermal	0.78	0.84	0.72	0.78	0.46	1.54	1.29
RF	PO	MS	0.72	0.83	0.68	0.73	0.33	1.72	1.38
RF	AO	All	0.89	0.89	0.86	0.88	0.55	3.18	2.44
RF	AO	MS, Thermal	0.61	0.76	0.51	0.51	0.26	4.11	3.15

Regarding the choice of regression versus classification for SWP prediction in the context of orchard irrigation management, classification models have some advantages over regression models. Irrigation strategies in real-world scenarios often adhere to a threshold-based framework (”irrigate” or ”do not irrigate”) wherein irrigation is performed once the SWP descends below a certain threshold. This binary decision-making process is intrinsically aligned with classification models, which predict discrete categories. Classifiers focus on categorizing data rather than determining exact values resulting in higher accuracy and more robustness against noise at the expense of less knowledge about the exact output values. They can provide better performance while trained on lower datasets. The deployment of machine learning models, particularly those trained on comprehensive datasets encompassing remote sensing and atmospheric information, could serve as a potential tool in discerning whether the SWP has breached a critical threshold. This could ultimately lead to more precise and timely irrigation decisions. The proposed approach embodies a practical and scalable solution to SWP prediction, enabling more sustainable and efficient water management practices within orchards.

4 CONCLUSIONS

This study offered a practical approach utilizing machine learning (ML) to evaluate orchard water status on a per-tree basis and enhance water management in orchards. Six ML models were utilized to classify stem water potential (SWP) using weather, thermal, and multispectral (MS) features, in pistachio orchard (PO) and almond orchard (AO). Additionally, random forest (RF) was used for classification and regression with different features. While most of ML classifiers used in this study provided %79 or higher performance in SWP classification, RF showed high performance in both PO and AO with %88 and %89 prediction accuracy, respectively. The feature importance report provided by the RF classifier accentuated the high influence of atmospheric features on SWP.

This dependency varied according to the level of water stress and type of crops. Weather features contributed to 48% and 77% of decisions in PO and AO, respectively. Therefore, leveraging such environmental variables that are both influential and easy to obtain, remain a necessity to achieve high performing predictive models. Thermal and MS features can provide valuable insight into water requirements of an orchard on a per-tree basis. Among those features, T_c played a more important role in SWP prediction in both crops. However, this significance was closely followed by OSAVI in pistachios and NDVI in almonds. NDRE exhibited lower importance in both crops. However, the gap between NDRE and NDVI importance was relatively smaller in the water-stressed AO compared to its difference with OSAVI in the non-stressed PO. The findings from this study suggest that the relative importance of features can be influenced by the prevailing water levels in the corresponding orchard. RF regression model predicted SWPs with highest accuracy when all weather, thermal, and MS inputs were involved resulting in $R^2 = 0.70$, $RMSE = 1.13\ bars$, MAE= 0.84 $bars$ in PO, and $R^2 = 0.55$, $RMSE = 3.18\ bars$, and $MAE = 2.44 bars$ in AO.

Future studies can focus on extending the application of the predictive models to other crops. Emphasis should be placed on the development of a model that can be utilized by end-users. This requires the adoption of features that are non-destructive, readily accessible, and reliant on remote sensing for facilitated individualized analysis. In this study, we used point measurements of leaf temperature to estimate average T_c for each tree under treatment. For enhanced scalability and to capture spatial temperature variations across individual trees and the entire orchard, thermal imaging using UAVs or UGVs is recommended. Incorporating machine learning is essential due to its capability in handling complex datasets and deriving meaningful insights. Given the proper quality and quantity of datasets, ML models are capable of capturing the intricate relationships between input features to predict an output. Therefore, input features can be broken down into their foundational components and be integrated with the ML models for training. For example, spectral bands and canopy temperature instead of VIs can directly be used for training the ML models. It is crucial to address the limitations posed by relying on single-season data which may not capture the variability across different growing conditions and locations. Expanding datasets across multiple seasons and regions potentially through collaborative databases or federated learning would enhance model generalizability leading to more reliable predictions. The power of artificial intelligence can be harnessed to unravel the complex relationship between variables that affect tree water status, which leads to better irrigation scheduling and more efficient water management in agriculture.

Acknowledgement

This work was supported primarily by the Internet of Things for Precision Agriculture (IoT4Ag) Engineering Research Center program of the National Science Foundation under NSF Cooperative Agreement No. EEC-1941529. Any Opinions, findings and conclusions or recommendations expressed in this material are those of the authors and do not necessarily reflect those of the National Science Foundation.

REFERENCES

Alizadeh, A., Toudeshki, A., Ehsani, R., Migliaccio, K., and Wang, D. (2021). Detecting tree water stress using a trunk relative water content measurement sensor. *Smart Agricultural Technology*, 1:100003. https://doi.org/10.1016/j.atech.2021.100003.

Ballester, C., Zarco-Tejada, P. J., Nicolás, E., Alarcón, J. J., Fereres, E., Intrigliolo, D. S., and Gonzalez-Dugo, V. (2018). Evaluating the performance of xanthophyll, chlorophyll and structure-sensitive spectral indices to detect water stress in five fruit tree species. *Precision agriculture*, 19:178–193. https://doi.org/10.1007/s11119-017-9512-y.

Ben-Gal, A., Agam, N., Alchanatis, V., Cohen, Y., Yermiyahu, U., Zipori, I., Presnov, E., Sprintsin, M., and Dag, A. (2009). Evaluating water stress in irrigated olives: correlation of soil water status, tree water status, and thermal imagery. *Irrigation science*, 27:367–376. https://doi.org/10.1007/s00271-009-0150-7.

Benos, L., Tagarakis, A. C., Dolias, G., Berruto, R., Kateris, D., and Bochtis, D. (2021). Machine learning in agriculture: A comprehensive updated review. *Sensors*, 21(11):3758. https://doi.org/10.3390/s21113758.

Carrasco-Benavides, M., Antunez-Quilobrán, J., Baffico-Hernández, A., Ávila-Sánchez, C., Ortega-Farías, S., Espinoza, S., Gajardo, J., Mora, M., and Fuentes, S. (2020). Performance assessment of thermal infrared cameras of different resolutions to estimate tree water status from two cherry cultivars: An alternative to midday stem water potential and stomatal conductance. *Sensors*, 20(12):3596. https://doi.org/10.3390/s20123596.

Carrasco-Benavides, M., Gonzalez Viejo, C., Tongson, E., Baffico-Hernández, A., Ávila-Sánchez, C., Mora, M., and Fuentes, S. (2022). Water status estimation of cherry trees using infrared thermal imagery coupled with supervised machine learning modeling. *Computers and Electronics in Agriculture*, 200(July). https://doi.org/10.1016/j.compag.2022.107256.

Celedón, J. M., Gil, P. M., Ferreyra, R., Maldonado, P., and Barrera, C. (2012). Sensitivity and variability of two plant water stress indicators: exploring criteria for choosing a plant monitoring method for avocado irrigation management. *Chilean Journal of Agricultural Research*, 72(3):379. http://dx.doi.org/10.4067/S0718-58392012000300012.

Chang, C.-C. and Lin, C.-J. (2011). Libsvm: a library for support vector machines. *ACM transactions on intelligent systems and technology (TIST)*, 2(3):1–27. https://doi.org/10.1145/1961189.1961199.

Delashmit, W. H., Manry, M. T., et al. (2005). Recent developments in multilayer perceptron neural networks. In *Proceedings of the seventh annual memphis area engineering and science conference, MAESC*, pages 1–15.

Egea, G., Padilla-Díaz, C. M., Martinez-Guanter, J., Fernández, J. E., and Pérez-Ruiz, M. (2017). Assessing a crop water stress index derived from aerial thermal imaging and infrared thermometry in super-high density olive orchards. *Agricultural Water Management*, 187:210–221. http://dx.doi.org/10.1016/j.agwat.2017.03.030.

Escriva-Bou, A., Hui, R., Maples, S., Medellín-Azuara, J., Harter, T., and Lund, J. (2020). Planning for groundwater sustainability accounting for uncertainty and costs: An application to california's central valley. *Journal of environmental management*, 264:110426. https://doi.org/10.1016/j.jenvman.2020.110426.

Espinoza, V., Bernacchi, L. A., Eriksson, M., Schiller, A., Hayden, A., and Viers, J. H. (2023). From fallow ground to common ground: Perspectives on future land uses in the san joaquin valley under sustainable groundwater management. *Journal of Environmental Management*, 333:117226. https://doi.org/10.1016/j.jenvman.2023.117226.

Fan, D., Su, X., Weng, B., Wang, T., and Yang, F. (2021). Research Progress on Remote Sensing Classification Methods for Farmland Vegetation. *AgriEngineering*, 3(4):971–989. https://doi.org/10.3390/agriengineering3040061.

García-Tejero, I., Durán-Zuazo, V. H., Arriaga, J., Hernández, A., Vélez, L. M., and Muriel-Fernández, J. L. (2012). Approach to assess infrared thermal imaging of almond trees under water-stress conditions. *Fruits*, 67(6):463–474. https://doi.org/10.1051/fruits/2012040.

Garofalo, S. P., Giannico, V., Costanza, L., Alhajj Ali, S., Camposeo, S., Lopriore, G., Pedrero Salcedo, F., and Vivaldi, G. A. (2023). Prediction of stem water potential in olive orchards using high-resolution planet satellite images and machine learning techniques. *Agronomy*, 14(1):1. https://doi.org/10.3390/agronomy14010001.

Gautam, D. and Pagay, V. (2020). A review of current and potential applications of remote sensing to study thewater status of horticultural crops. *Agronomy*, 10(1). https://doi.org/10.3390/agronomy10010140.

Giménez-Gallego, J., González-Teruel, J. D., Soto-Valles, F., Jiménez-Buendía, M., Navarro-Hellín, H., and Torres-Sánchez, R. (2021). Intelligent thermal image-based sensor for affordable measurement of crop canopy temperature. *Computers and Electronics in Agriculture*, 188:106319. https://doi.org/10.1016/j.compag.2021.106319.

Gonzalez-Dugo, V., Goldhamer, D., Zarco-Tejada, P. J., and Fereres, E. (2015). Improving the precision of irrigation in a pistachio farm using an unmanned airborne thermal system. *Irrigation science*, 33:43–52. https://doi.org/10.1007/s00271-014-0447-z.

Gonzalez-Dugo, V., Zarco-Tejada, P., Berni, J. A., Suarez, L., Goldhamer, D., and Fereres, E. (2012). Almond tree canopy temperature reveals intra-crown variability that is water stress-dependent. *Agricultural and Forest Meteorology*, 154:156–165. https://doi.org/10.1016/j.agrformet.2011.11.004.

González-Dugo, V., Zarco-Tejada, P. J., and Fereres, E. (2014). Applicability and limitations of using the crop water stress index as an indicator of water deficits in citrus orchards. *Agricultural and forest meteorology*, 198:94–104. https://doi.org/10.1016/j.agrformet.2014.08.003.

Gutiérrez-Gordillo, S., González-Santiago, J. d. l. G., Trigo-Córdoba, E., Rubio-Casal, A. E., García-Tejero, I. F., and Egea, G. (2021). Monitoring of emerging water stress situations by thermal and vegetation indices in different almond cultivars. *Agronomy*, 11(7). https://doi.org/10.3390/agronomy11071419.

Hong, C., Mueller, N. D., Burney, J. A., Zhang, Y., AghaKouchak, A., Moore, F. C., Qin, Y., Tong, D., and Davis, S. J. (2020). Impacts of ozone and climate change on yields of perennial crops in california. *Nature Food*, 1(3):166–172. https://doi.org/10.1038/s43016-020-0043-8.

Idso, S., Jackson, R., Pinter Jr, P., Reginato, R., and Hatfield, J. (1981). Normalizing the stress-degree-day parameter for environmental variability. *Agricultural meteorology*, 24:45–55. https://doi.org/10.1016/0002-1571(81)90032-7.

Jafarbiglu, H. and Pourreza, A. (2022). A comprehensive review of remote sensing platforms, sensors, and applications in nut crops. *Computers and Electronics in Agriculture*, 197:106844. https://doi.org/10.1016/j.compag.2022.106844.

Kagan, C. R., Arnold, D. P., Cappelleri, D. J., Keske, C. M., and Turner, K. T. (2022). Special report: The internet of things for precision agriculture (iot4ag). *Computers and Electronics in Agriculture*, 196:106742. https://doi.org/10.1016/j.compag.2022.106742.

Katimbo, A., Rudnick, D. R., DeJonge, K. C., Lo, T. H., Qiao, X., Franz, T. E., Nakabuye, H. N., and Duan, J. (2022). Crop water stress index computation approaches and their sensitivity to soil water dynamics. *Agricultural Water Management*, 266:107575. https://doi.org/10.1016/j.agwat.2022.107575.

Kirnak, H., Irik, H., and Unlukara, A. (2019). Potential use of crop water stress index (cwsi) in irrigation scheduling of drip-irrigated seed pumpkin plants with different irrigation levels. *Scientia Horticulturae*, 256:108608. https://doi.org/10.1016/j.scienta.2019.108608.

Lampinen, B., Shackel, K., and Metcalf, S. (2015). Using midday stem water potential to refine irrigation scheduling in almond. *Dep. of Plant Sciences, UC Davis.[cit. 2015-01]. http://ucmanagedrought. ucdavis. edu/Agriculture/Crop_Irrigation_Strategies/Walnuts*.

Liakos, K. G., Busato, P., Moshou, D., Pearson, S., and Bochtis, D. (2018). Machine learning in agriculture: A review. *Sensors (Switzerland)*, 18(8):1–29. https://doi.org/10.3390/s18082674.

Liu, L., Gao, X., Ren, C., Cheng, X., Zhou, Y., Huang, H., Zhang, J., and Ba, Y. (2022). Applicability of the crop water stress index based on canopy–air temperature differences for monitoring water status in a cork oak plantation, northern china. *Agricultural and Forest Meteorology*, 327:109226. https://doi.org/10.1016/j.agrformet.2022.109226.

Loggenberg, K., Strever, A., Greyling, B., and Poona, N. (2018). Modelling water stress in a shiraz vineyard using hyperspectral imaging and machine learning. *Remote Sensing*, 10(2):202. https://doi.org/10.3390/rs10020202.

Marques Ramos, A. P., Prado Osco, L., Elis Garcia Furuya, D., Nunes Gonçalves, W., Cordeiro Santana, D., Pereira Ribeiro Teodoro, L., Antonio da Silva Junior, C., Fernando Capristo-Silva, G., Li, J., Henrique Rojo Baio, F., Marcato Junior, J., Eduardo Teodoro, P., and Pistori, H. (2020). A random forest ranking approach to predict yield in maize with uav-based vegetation spectral indices. *Computers and Electronics in Agriculture*, 178(September):105791. https://doi.org/10.1016/j.compag.2020.105791.

Martínez-Peña, R., Vélez, S., Vacas, R., Martín, H., and Álvarez, S. (2023). Remote sensing for sustainable pistachio cultivation and improved quality traits evaluation through thermal and non-thermal uav vegetation indices. *Applied Sciences*, 13(13):7716. https://doi.org/10.3390/app13137716.

Medellín-Azuara, J., Escriva-Bou, A., Rodríguez-Flores, J. M., Cole, S. A., Abatzoglou, J., Viers, J. H., Santos, N., Summer, D. A., Medina, C., Arévalo, R., et al. (2022). Economic impacts of the 2020–22 drought on california agriculture.

Messikh, N., Bousba, S., and Bougdah, N. (2017). The use of a multilayer perceptron (mlp) for modelling the phenol removal by emulsion liquid membrane. *Journal of Environmental Chemical Engineering*, 5(4):3483–3489. https://doi.org/10.1016/j.jece.2017.06.053.

Meyers, J. N., Kisekka, I., Upadhyaya, S. K., and Michelon, G. K. (2019). Development of an artificial neural network approach for predicting plant water status in almonds. *Transactions of the ASABE*, 62(1):19–32.

Millán, S., Campillo, C., Casadesús, J., Pérez-Rodríguez, J. M., and Prieto, M. H. (2020). Automatic irrigation scheduling on a hedgerow olive orchard using an algorithm of water balance readjusted with soil moisture sensors. *Sensors*, 20(9):2526. https://doi.org/10.3390/s20092526.

Mobe, N., Dzikiti, S., Volschenk, T., Zirebwa, S., Ntshidi, Z., Midgley, S., Steyn, W., Lötze, E., Mpandeli, S., and Mazvimavi, D. (2020). Using sap flow data to assess variations in water use and water status of apple orchards of varying age groups in the western cape province of south africa. *Water SA*, 46(2):213–224. https://doi.org/10.17159/wsa/2020.v46.i2.8246.

Ntshidi, Z., Dzikiti, S., Mazvimavi, D., and Mobe, N. T. (2023). Effect of different irrigation systems on water use partitioning and plant water relations of apple trees growing on deep sandy soils in the mediterranean climatic conditions, south africa. *Scientia Horticulturae*, 317:112066. https://doi.org/10.1016/j.scienta.2023.112066.

Ohana-Levi, N., Zachs, I., Hagag, N., Shemesh, L., and Netzer, Y. (2022). Grapevine stem water potential estimation based on sensor fusion. *Computers and Electronics in Agriculture*, 198(February):107016. https://doi.org/10.1016/j.compag.2022.107016.

Pagano, A., Amato, F., Ippolito, M., De Caro, D., Croce, D., Motisi, A., Provenzano, G., and Tinnirello, I. (2023). Machine learning models to predict daily actual evapotranspiration of citrus orchards under regulated deficit irrigation. *Ecological Informatics*, 76:102133. https://doi.org/10.1016/j.ecoinf.2023.102133.

Pedregosa, F., Varoquaux, G., Gramfort, A., Michel, V., Thirion, B., Grisel, O., Blondel, M., Prettenhofer, P., Weiss, R., Dubourg, V., Vanderplas, J., Passos, A., Cournapeau, D., Brucher, M., Perrot, M., and Duchesnay, E. (2011). Scikit-learn: Machine learning in Python. *Journal of Machine Learning Research*, 12:2825–2830. https://www.jmlr.org/papers/v12/pedregosa11a.html.

Peters, E. B., McFadden, J. P., and Montgomery, R. A. (2010). Biological and environmental controls on tree transpiration in a suburban landscape. *Journal of Geophysical Research: Biogeosciences*, 115(G4). https://doi.org/10.1029/2009JG001266.

Quinlan, J. R. (1993). C 4.5: Programs for machine learning. *The Morgan Kaufmann Series in Machine Learning*.

Ray, S. (2019). A quick review of machine learning algorithms. In *2019 International conference on machine learning, big data, cloud and parallel computing (COMITCon)*, pages 35–39. IEEE. https://doi.org/10.1109/COMITCon.2019.8862451.

Rish, I. et al. (2001). An empirical study of the naive bayes classifier. In *IJCAI 2001 workshop on empirical methods in artificial intelligence*, volume 3, pages 41–46.

Romero, M., Luo, Y., Su, B., and Fuentes, S. (2018). Vineyard water status estimation using multispectral imagery from an UAV platform and machine learning algorithms for irrigation scheduling management. *Computers and Electronics in Agriculture*, 147(January):109–117. https://doi.org/10.1016/j.compag.2018.02.013.

Savchik, P., Nocco, M., and Kisekka, I. (2024). Mapping almond stem water potential using machine learning and multispectral imagery. *Irrigation Science*, pages 1–16. https://doi.org/10.1007/s00271-024-00932-8.

Sun, A. Y. and Scanlon, B. R. (2019). How can big data and machine learning benefit environment and water management: a survey of methods, applications, and future directions. *Environmental Research Letters*, 14(7):073001. https://doi.org/10.1088/1748-9326/ab1b7d.

Taunk, K., De, S., Verma, S., and Swetapadma, A. (2019). A brief review of nearest neighbor algorithm for learning and classification. In *2019 international conference on intelligent computing and control systems (ICCS)*, pages 1255–1260. IEEE. https://doi.org/10.1109/ICCS45141.2019.9065747.

Testi, L., Goldhamer, D., Iniesta, F., and Salinas, M. (2008). Crop water stress index is a sensitive water stress indicator in pistachio trees. *Irrigation science*, 26:395–405. https://doi.org/10.1007/s00271-008-0104-5.

Vera, J., Conejero, W., Conesa, M. R., and Ruiz-Sánchez, M. C. (2019). Irrigation factor approach based on soil water content: A nectarine orchard case study. *Water*, 11(3):589. https://doi.org/10.3390/w11030589.

Virnodkar, S. S., Pachghare, V. K., Patil, V. C., and Jha, S. K. (2020). *Remote sensing and machine learning for crop water stress determination in various crops: a critical review*, volume 21. Springer US. https://doi.org/10.1007/s11119-020-09711-9.

Zhao, T., Stark, B., Chen, Y. Q., Ray, A. L., and Doll, D. (2017). Challenges in Water Stress Quantification Using Small Unmanned Aerial System (sUAS): Lessons from a Growing Season of Almond. *Journal of Intelligent and Robotic Systems: Theory and Applications*, 88(2-4):721–735. https://doi.org/10.1109/ICUAS.2016.7502642.

Zhou, J.-J., Zhang, Y.-H., Han, Z.-M., Liu, X.-Y., Jian, Y.-F., Hu, C.-G., and Dian, Y.-Y. (2021). Evaluating the performance of hyperspectral leaf reflectance to detect water stress and estimation of photosynthetic capacities. *Remote Sensing*, 13(11):2160. https://doi.org/10.3390/rs13112160.